# Classical limit states of the helium atom

J. A. West,[1,2] Z. D. Gaeta,[1,3] and C. R. Stroud, Jr.[1,2]
[1]*The Institute of Optics, University of Rochester, Rochester, New York 14627*
[2]*Rochester Theory Center for Optical Science and Engineering, University of Rochester, Rochester, New York 14627*
[3]*Chemistry Department, Cornell University, Ithaca, New York 14853*
(Received 31 January 1997)

The techniques of Rydberg electronic wave packets are used to explore the classical limit states of helium. A class of *shape-preserving* orbits is studied under the classical adiabatic approximation that separates the dynamics of the two electrons. These states form the classical basis for two-electron wave packet states whose hydrogenic counterparts are shown to be elliptic states in the presence of a rotating electric field. [S1050-2947(98)10906-X]

PACS number(s): 31.25.Jf, 31.50.+w, 32.80.Rm, 46.10.+z

## I. INTRODUCTION

The classical simplicity and intuitive appeal of Bohr's atomic model have given the classical hydrogen atom an important and pervasive role in atomic physics. Even today, the Bohr model remains as a cornerstone underlying quantum mechanics. However, the precise role of this classical foundation has been debated since the early days of quantum theory. Recently, a series of experimental and theoretical studies has sought to explore the classical limit of quantum mechanics using Rydberg electron wave packets [1]. These studies of hydrogenlike atoms have allowed us to understand some of the essential differences between the quantum mechanical atom and its more familiar classical counterpart.

The logical progression of the hydrogenic studies is to extend them to include planetary atoms with multiple valence electrons [2–6]. However, even for the simplest such atom, helium, this extension is nontrivial because the old quantum theory of Bohr was never successfully modified to include helium. Early in this century a considerable effort was made to develop a classical model for helium, but no stable planetary orbits were found [see Figs. 1(a) and 1(b)]. By 1920 Bohr had concluded that for stability, one must allow for ''possibilities of more complicated motions,'' [7] but before these possibilities could be explored, classical atomic physics was abandoned in the wake of wave mechanics and classical helium was put aside. However, the success of the hydrogenic wave packet studies and recent progress in semiclassical dynamics has once again revived interest in the classical limit of multielectron systems [9–11].

In this paper we discuss an approach that relies heavily on hydrogenic wave packet models while including effects that are unique to multielectron atoms. If the effects of a second valence electron are considered, the resulting dynamics, both classical and quantum mechanical, is in general unstable. The doubly excited system decays rapidly as a result of autoionization, with one electron ejected and the other falling back to an ionic ground state [12]. However, some isolated classes of classical two-electron orbits [see Figs. 1(c) and 1(d)] are known to be stable despite the fact that their energy is above the one-electron ionization threshold [11,13–15]. Studies of wave packet states based on such ''planetary'' orbits will help to extend our understanding of the classical limit of quantum dynamics involving multiple electrons.

Stable two-electron states are very attractive from the experimental point of view because they provide an environment in which electron correlation can be studied over long periods of time. Planetary atom states [2] are those in which the electrons are excited to asymmetric double Rydberg states (i.e., the radial expectation values are unequal, $\langle r_1 \rangle \ll \langle r_2 \rangle$). In a very general way, the correlations in these planetary states can be ascribed to the radial and angular dynamics of the classical electron-electron interaction [16]. It is the angular correlation that is of interest in the orbits that we will discuss in this paper. The polarizing effect of the outer electron leads to states whose classical counterparts exhibit a coupling between the outer electron and the orbital parameters of the inner electron.

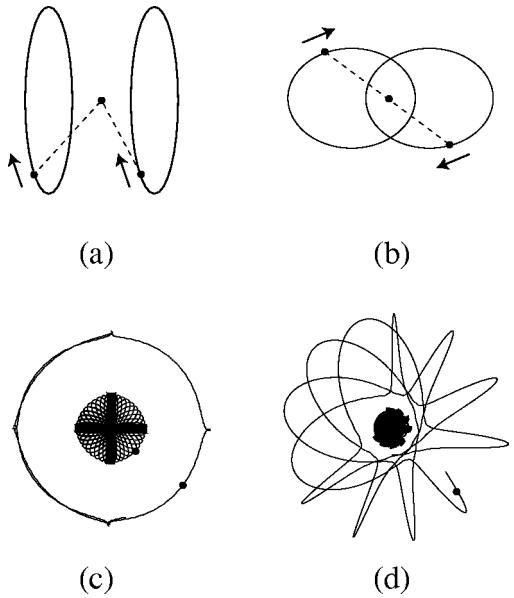


FIG. 1. A pictorial survey of some classical helium orbits. The two-electron trajectories shown in (a) and (b) are highly symmetric unstable orbits which were studied in an attempt to extend the Bohr model [3,7,8]. The orbits shown in (c) and (d) are stable orbits in which the dynamics of the individual electrons is quite dissimilar. In these orbits it is difficult to resolve the rapid motion of the inner electron.

 © 1998 The American Physical Society

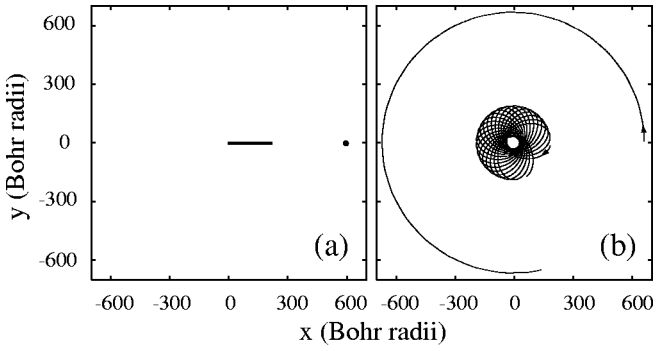


FIG. 2. Numerical simulations of two-electron orbits in helium. (a) In the classical frozen planet configuration the two electrons are found in a collinear arrangement on the same side of the nucleus (which lies at the origin). For this orbit $Z_{\mathrm{eff}}$ and the total angular momentum are zero. (b) The major axis of the inner electron's orbit adiabatically follows the outer electron in a shape-invariant orbit for which $Z_{\mathrm{eff}}=0.5$ and the total angular momentum is nonzero.

We will demonstrate that the dynamical picture of a broad class of these planetary orbits can be greatly simplified by reduction to two coupled single-electron models. This simplification is accomplished with the help of an adiabatic approximation, which can be applied in the case in which one of the electrons is more highly excited than the other [17]. For even a modest difference in excitation energies the more tightly bound inner electron will complete many revolutions per single revolution of the outer electron. This difference in time scales plays a very important role in the determination of the effect of the electron-electron interaction.

This interaction can be divided into two components describing the effect of each electron on the other. The slowly moving outer electron cannot respond to the rapidly changing repulsive Coulomb force due to the inner electron. Instead, it experiences a core screening which, when averaged over the entire orbit of the inner electron, can be replaced by an effective core charge $Z_{\mathrm{eff}}$ in a hydrogenic system. This classical outer electron is represented quantum mechanically by a circular orbit wave packet [18] moving about the screened core. To model the averaged effect of the outer electron on the inner electron, we can replace the outer electron by an equivalent electric field $E_{\mathrm{eff}}$ in a manner similar to that first suggested by Bohr [7] for dc electric fields and later evidenced in the experiments of Eichmann *et al.* [19]. In contrast to the dc fields results, the orbits discussed in this paper require an equivalent rotating field. The resulting classical model with this effective electric field has a quantum-mechanical analog that we will show to be an elliptic state or angular wave packet. Thus we develop two coupled one-electron systems that self-consistently include the effects of both electrons and whose counterparts in quantum mechanics are wave packet states.

In Fig. 2 are shown two orbits for which such an adiabatic separation of the dynamics is appropriate. Extensive studies [5,10,11,14,17,20–22] of the unusual *frozen planet configurations* shown in Fig. 2(a) were motivated by the experiment of Eichmann *et al.* [19] in barium. The inner electron travels in a linear orbit, spending most of the time near the outer turning point and completely shielding the core from the outer electron. In this paper we are concerned with a broad class of two-electron configurations of which the frozen planet is a limiting case. In the general case of this kind the initial trajectory of the inner electron is an arbitrary ellipse, while the outer electron initially travels in a high-angular-momentum orbit in the same plane as that of the inner electron. An example of such an orbit is shown in Fig. 2(b). The shielding of the core by the elliptic inner orbit is incomplete and the outer electron moves slowly in a circle. Orbits such as those in Fig. 2 are remarkable because there is no net exchange of angular momentum between the electrons. A consequence of this is that, although the inner orbit precesses, its shape does not change in time. We will refer to this class of orbits as *shape preserving*.

## II. CLASSICAL ADIABATIC MODEL

We begin our formal analysis by treating the case of a single classical electron orbiting an atomic core with charge $Z$ in the presence of a weak circularly polarized electric field. The goal is to find the conditions under which a single-electron orbit in a rotating electric field can mimic the behavior of the inner orbit shown in Fig. 2(b). The signature of this behavior is simply a precession of a shape-preserving orbit.

The adiabatic analysis is a generalization of the static field result first obtained by Bohr [7] and revived more recently in the study of Rydberg atoms [23–27]. As in the case of the static field, the interesting dynamics of the system is contained entirely in the evolution of the time-averaged orbital parameters, and not in the rapidly varying position and momentum, $\mathbf{r}$ and $\mathbf{p}$. We require that the field be weak and slowly varying so that the time scale of the field-induced dynamics is much longer than the orbital or Kepler period, $T_k$, of the electronic motion. This allows us to average the orbital parameters over a Kepler period using the adiabatic approximation well known in physics [28].

The orbital parameters of interest are the angular momentum, $\mathbf{L}=\mathbf{r}\times\mathbf{p}$, and the scaled Runge-Lenz vector

$$\mathbf{A}=\frac{n}{Z}\left(\mathbf{p}\times\mathbf{L}-\frac{Z\mathbf{r}}{r}\right). \tag{1}$$

(We use atomic units throughout the paper.) The scaled Runge-Lenz vector is a constant of the field-free motion and lies antiparallel to the major axis of the orbit and perpendicular to the angular momentum vector. Its magnitude is equal to $n\epsilon$ where $\epsilon$ is the eccentricity of the orbit,

$$\epsilon=\sqrt{1-\frac{|\mathbf{L}|^2}{n^2}}, \tag{2}$$

and $n$ corresponds to the energy $\mathcal{E}=-Z^2/(2n^2)$. The time evolution of $\mathbf{L}$ and $\mathbf{A}$ is found by differentiating the above equations and by replacing the expressions for $\dot{\mathbf{r}}$ and $\dot{\mathbf{p}}$ with Hamilton's equations of motion. The Hamiltonian in the presence of the field is

$$H=H_0+\mathbf{r}\cdot\mathbf{E}(t)=\frac{p^2}{2}-\frac{Z}{r}+\mathbf{r}\cdot\mathbf{E}(t), \tag{3}$$

where $\mathbf{E}(t)$ is an electric field whose amplitude varies slowly compared to the orbital frequency. The rapid oscillations due

to the motion of the inner electron are removed by averaging the equations for $\dot{\mathbf{L}}$ and $\dot{\mathbf{A}}$ over one orbital period $T_k$. The resulting equations are

$$\langle \dot{\mathbf{A}} \rangle_{T_k} = -\frac{3n}{2Z} \langle \mathbf{E} \rangle_{T_k} \times \langle \mathbf{L} \rangle_{T_k} = -\boldsymbol{\omega}_s \times \langle \mathbf{L} \rangle_{T_k},$$
$$\langle \dot{\mathbf{L}} \rangle_{T_k} = -\frac{3n}{2Z} \langle \mathbf{E} \rangle_{T_k} \times \langle \mathbf{A} \rangle_{T_k} = -\boldsymbol{\omega}_s \times \langle \mathbf{A} \rangle_{T_k}, \tag{4}$$

where $\boldsymbol{\omega}_s$ is the Stark frequency vector pointing in the direction of the applied field.

If $\mathbf{E}$ is an electrostatic field in the plane of the orbit Eqs. (4) describe a well-known Stark oscillation of the angular momentum and the eccentricity of the ellipse with frequency $\omega_s = 3nE/(2Z)$ [7]. The only orbit that remains unchanged by the field is the linear orbit aligned with the field, whose quantum-mechanical counterpart, the extreme Stark state, is an eigenstate of the atom-plus-field Hamiltonian.

The dynamics of $\langle \mathbf{L} \rangle_{T_k}$ and $\langle \mathbf{A} \rangle_{T_k}$ are more complex when the applied field is a circularly polarized electric field rotating slowly with frequency $\boldsymbol{\omega}_r = \omega_r \hat{z}$:

$$\mathbf{E}(t) = E[\cos(\omega_r t)\hat{\mathbf{x}} + \sin(\omega_r t)\hat{\mathbf{y}}]. \tag{5}$$

If $\omega_r \ll 2\pi/T_k$, the time averages of $\dot{\mathbf{L}}$ and $\dot{\mathbf{A}}$ are still valid and the equations can be simplified with the introduction of an angular momentum vector $\tilde{\mathbf{L}}(t)$ and a scaled Runge-Lenz vector $\tilde{\mathbf{A}}(t)$ rotating with the electric field

$$\tilde{\mathbf{L}}(t) = R(t)\langle \mathbf{L}(t) \rangle_{T_k},$$
$$\tilde{\mathbf{A}}(t) = R(t)\langle \mathbf{A}(t) \rangle_{T_k}, \tag{6}$$
$$R(t) = \begin{pmatrix} \cos(\omega_r t) & \sin(\omega_r t) & 0 \\ -\sin(\omega_r t) & \cos(\omega_r t) & 0 \\ 0 & 0 & 1 \end{pmatrix}.$$

Using the coordinates defined by the orientation of the field in Eq. (5), the symmetry of the interaction divides the orbital parameters into two uncoupled vectors $\boldsymbol{\lambda}_\parallel = (\tilde{A}_x, \tilde{A}_y, \tilde{L}_z)$ and $\boldsymbol{\lambda}_\perp = (\tilde{L}_x, \tilde{L}_y, \tilde{A}_z)$. Orbits whose angular momenta are parallel to $\boldsymbol{\omega}_r$ are described by $\boldsymbol{\lambda}_\parallel$, while $\boldsymbol{\lambda}_\perp$ describes those orbits whose angular momenta lie in the plane of rotation. Using Eqs. (4) it is easily shown that these vectors evolve according to

$$\frac{d}{dt}\boldsymbol{\lambda}_\perp = -\boldsymbol{\Omega} \times \boldsymbol{\lambda}_\perp, \tag{7}$$

$$\frac{d}{dt}\boldsymbol{\lambda}_\parallel = -\boldsymbol{\Omega} \times \boldsymbol{\lambda}_\parallel, \tag{8}$$

where $\boldsymbol{\Omega} = \boldsymbol{\omega}_s + \boldsymbol{\omega}_r$. Equations (7) and (8) describe precession about $\boldsymbol{\Omega}$ in the rotating frame. However, if either vector $\boldsymbol{\lambda}_\parallel$ or $\boldsymbol{\lambda}_\perp$ is initially parallel or antiparallel to $\boldsymbol{\Omega}$, there will be no precession and the initial vector will remain unchanged. In the laboratory frame the orbit rotates with the field without changing its shape. It is these shape-preserving orbits that are of interest in describing the two-electron orbits of Fig. 2.

In general, shape-preserving orbits exist in single-electron systems as long as the initial angular momentum and Runge-Lenz vectors lie in the plane defined by $\boldsymbol{\omega}_s$ and $\boldsymbol{\omega}_r$. However, for reasons of symmetry, this model is only useful for classical two-electron systems in which both orbits lie in the same plane [29]. The orbits shown in Fig. 2 satisfy this requirement and can be modeled by single-electron orbits belonging to the $\boldsymbol{\lambda}_\parallel$ class. Simple precession in the laboratory frame is represented by a shape-preserving orbit in the rotating frame. For orbits lying in the plane of rotation, Eq. (8) is easily solved:

$$\tilde{L}_z(t) = \tilde{L}_z(0) - \frac{\omega_s}{\Omega}\tilde{A}_y(0)\sin(\Omega t) + \frac{\omega_s \gamma}{\Omega^2}[\cos(\Omega t) - 1],$$
$$\tilde{A}_x(t) = \tilde{A}_x(0) + \frac{\omega_r}{\Omega}\tilde{A}_y(0)\sin(\Omega t) - \frac{\omega_r \gamma}{\Omega^2}[\cos(\Omega t) - 1], \tag{9}$$
$$\tilde{A}_y(t) = \tilde{A}_y(0)\cos(\Omega t) + \frac{\gamma}{\Omega}\sin(\Omega t),$$

where $\Omega = |\boldsymbol{\Omega}| = \sqrt{\omega_r^2 + \omega_s^2}$ is a generalized frequency and $\gamma$ is a parameter defined by

$$\gamma = \dot{\tilde{A}}_y(0) = \omega_s \tilde{L}_z(0) - \omega_r \tilde{A}_x(0). \tag{10}$$

For a shape-preserving solution, the initial vector $\boldsymbol{\lambda}_\parallel(0)$ lies along $\boldsymbol{\Omega}$ requiring

$$\tilde{A}_y(0) = 0, \tag{11}$$

$$\gamma = 0. \tag{12}$$

The first of these conditions simply states that the orbit must be aligned initially with the field. The second condition describes a balance between the rotation of the electric field and the Stark evolution of the orbital parameters. When $\gamma = 0$ these effects cancel to produce a simple precession of the orbit analogous to that found in two-electron orbits. For an elliptical orbit aligned with the field, having initial angular momentum $l$ and eccentricity $\epsilon$, this condition on $\gamma$ can be rewritten as

$$\omega_r = -\omega_s \frac{l}{n\epsilon}. \tag{13}$$

Any choice of orbit can be made shape invariant over a wide range of field strengths and frequencies related by Eq. (13). When rewritten as Eq. (13) it is clear that the handedness of the orbital motion is opposite to that of the rotating field. In two-electron orbits this condition requires that the electrons orbit the nucleus in opposite directions. Kalinski [30] has shown that if the axis of the inner orbit is aligned antiparallel to the radius vector of the outer electron, a limited range of solutions is allowed in which the two electrons orbit in the same direction.

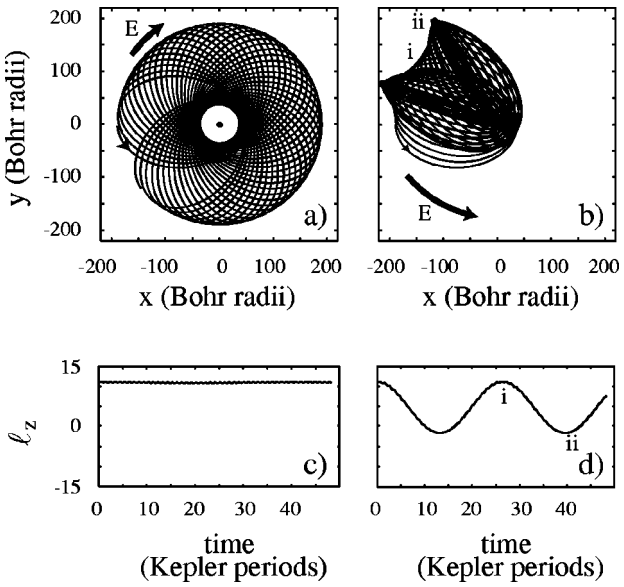


FIG. 3. The Stark evolution of the electron trajectory in a classical hydrogenic atom (with $Z=2, n=15, l=11$) in a rotating electric field. Initially, the electric field lies along the major axis of the orbital ellipse. (a) When $\gamma$ is zero ($\omega_s = 2\times10^{-5}$ s$^{-1}$ and $\omega_r = 2.16\times10^{-5}$ s$^{-1}$), the major axis of the orbit adiabatically follows the field. (b) In this orbit for which $\gamma$ is nonzero ($\omega_s = 2\times10^{-5}$ s$^{-1}$, $\omega_r = -4\times10^{-5}$ s$^{-1}$, and $\gamma = -6.28\times10^{-5}$ s$^{-1}$), the field rotates in the *opposite* direction at twice the frequency and the major axis of the orbit does *not* follow the field. The corresponding angular momenta as functions of time are shown in (c) and (d). The labels (i, ii) indicate the angular momentum for various points on the trajectory in (b).

In Fig. 3 we show two orbits in the presence of a rotating field. When $\gamma=0$, Eqs. (9) become time independent and the shape of the orbit remains unchanged in the rotating frame as the major axis of the ellipse adiabatically follows the field. In the laboratory frame this motion appears as the slow precession of the orbit shown in Fig. 3(a). This effect produced by a rotating electric field will allow us to model part of the two-electron dynamics with this simple single-electron model. In the limiting case $\omega_r \to 0$ it follows that the only shape-invariant orbit has angular momentum $l \to 0$, making $\gamma$ trivially zero. This result reaffirms the previous observation, that the linear orbit is stationary in an electrostatic field.

The dynamics of the orbit shown in Fig. 3(b) appears to be much more complicated when $\gamma$ does not equal zero. However, Eqs. (9) reveal that the behavior that looks quite complicated in the trajectory can be understood simply in terms of an oscillating angular momentum as we see in Fig. 3(d). This behavior is also evident in the two-electron orbits that are examined in the following section. In this case it can be interpreted in terms of an exchange of angular momentum between the two electrons.

We point out that, despite the similarity of this situation to that of a Trojan wave packet [31,32], the physics is quite different. Briefly, a Trojan wave packet is formed when a circular state is placed in a circularly polarized electric field rotating at the Kepler frequency. The field couples the initial state to neighboring circular states forming a wave packet that does not exhibit the spreading and interference associated with field-free circular-orbit wave packets [18]. The stabilization of the Trojan wave packets represents a balance between the applied field and the dispersion inherent between the energy levels of different $n$ manifolds. In the case of the shape-preserving orbits discussed in this paper, a wave packet representation would involve states from the same $n$ manifold and hence no dispersion. The stabilization in this case is a balance between the two field-generated effects. This type of stabilization is of limited interest in single-electron atoms but is important in discussions of two-electron dynamics, as we will see in the following section.

A close connection between the Trojan wave packets and the multielectron dynamics described here was recently proposed for rotating molecular systems that have a large electric dipole moment [33]. The role of the rotating electric field is replaced by the presence of the rotating dipole moment producing a system that is functionally identical to that of the atomic Trojan wave packets.

## III. CLASSICAL MODEL OF DYNAMICAL SCREENING IN TWO-ELECTRON ATOMS

It now remains to be shown that the model of a single-electron atom in a rotating field can be used to predict the behavior of the two-electron system. Two parameters must be calculated: the effective core charge seen by the outer electron and the effective rotating electric field experienced by the inner electron. The shape-invariant precessing orbits are found by coupling these quantities together under the condition $\gamma=0$.

The motion of the outer electron is modeled by a circular orbit around a core of charge $Z_{\rm eff}$. We characterize this orbit with $n_2$ and $l_2=n_2$, and by an orbital period $T_2 = 2\pi n_2^3/Z_{\rm eff}^2$. The inner electron is in an elliptic orbit about a core of $Z=2$ with $n_1$, $l_1$, and eccentricity $\epsilon_1$. The Bohr radius of this orbit is given by $a_1 = n_1^2/Z$. The effective radial force experienced by the outer electron, averaged over the motion of the inner electron, is

$$F_{\rm eff} = \frac{Z_{\rm eff}(r_2)}{r_2^2} = -\left\langle \frac{r_2 - r_1\cos\theta_1}{|\mathbf{r}_2-\mathbf{r}_1|^3} \right\rangle_{T_1} + \frac{2}{r_2^2}. \qquad (14)$$

Although Eq. (14) has an analytic solution in terms of elliptic integrals we will express its solution in terms of a multipole expansion in powers of $r_1/r_2$:

$$Z_{\rm eff}(r_2) = 1 - \frac{3a_1\epsilon_1}{r_2} - \frac{3a_1^2}{4r_2^2}(1+9\epsilon_1^2) + O\left(\frac{a_1}{r_2}\right)^3. \qquad (15)$$

For helium ($Z=2$) the ratio $r_2/a_1 > 5.4$ [see Fig. 4(a)] for all values of $\epsilon_1$, and only the first few terms of the series (15) are necessary. In the case of a linear inner-electron orbit ($\epsilon_1=1$) the expansion for the effective potential coincides with the one in Ref. [17].

To complete the analogy of our two-electron model to a single-electron atom in a rotating field, we calculate the effective field experienced by the inner electron,

$$E_{\rm eff} = \left\langle \frac{r_2 - r_1\cos\theta_1}{|\mathbf{r}_2-\mathbf{r}_1|^3} \right\rangle_{T_1}, \qquad (16)$$

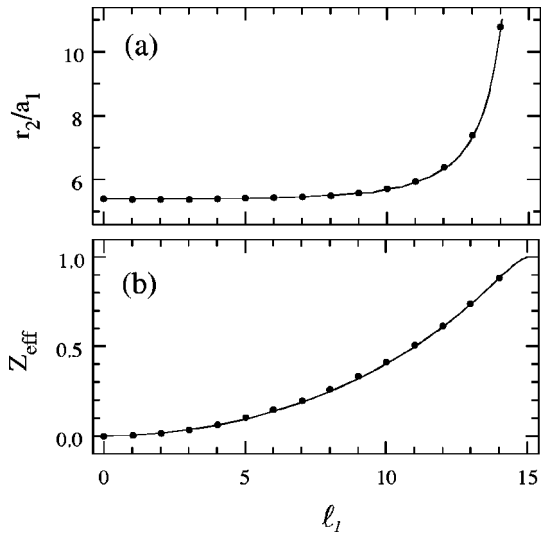


FIG. 4. The radial position (in units of $a_1$) and the effective charge seen by the outer electron orbiting an inner electron with $n_1=15$. The line in (a) is the solution to equation (18) and these values of $r_2$ are then substituted into (15) to give the effective charge shown in (b). The points on both plots were calculated by numerically integrating the equations of motion for the classical helium problem with a nucleus of infinite mass. In the limit of a linear inner orbit, $l_1 \rightarrow 0$, the inner electron completely screens the nucleus.

which may also be expressed in terms of a multipole expansion in powers of $r_1/r_2$:

$$E_{\mathrm{eff}}(r_2)=\frac{1}{r_2^2}\left[1+\frac{3a_1\epsilon_1}{r_2}+\frac{3a_1^2}{4r_2^2}(1+9\epsilon_1^2)+O\left(\frac{a_1}{r_2}\right)^3\right]. \tag{17}$$

Equation (13) provides the condition for a shape-invariant inner-electron orbit. In the coupled single-electron models the inner electron interacts with an electric field $E_{\mathrm{eff}}$, which rotates with frequency $\omega_r=2\pi/T_2$, while the outer electron sees a core of charge $Z_{\mathrm{eff}}$. Equations (13), (15), and (17) can be combined into an equation in $r_2$,

$$\frac{3E_{\mathrm{eff}}(r_2)}{2Z}=\frac{\epsilon_1}{l_1}\sqrt{\frac{Z_{\mathrm{eff}}(r_2)}{r_2^3}}, \tag{18}$$

which is solved numerically to find the radius of the outer electron that assures that the orbit of the inner electron does not change shape.

In Fig. 4 are shown plots of the values of $r_2$ and $Z_{\mathrm{eff}}$, predicted by the coupled one-electron models, as functions of the eccentricity of the inner orbit. In the same figure are shown the corresponding values from numerical simulations obtained by integrating the classical equations of motion for the full two-electron problem. The latter results were obtained by searching for a configuration that minimized the exchange of angular momentum between the electrons. The agreement between the approximate analytic result and the full numerical simulation is extremely good. As the inner orbit becomes more eccentric the degree of core shielding increases, reducing the effective charge $Z_{\mathrm{eff}}$ to zero. This is the limit of the frozen planet configurations. In the other limit, the orbit of the inner electron becomes circular and the screened core charge approaches unity. Although in this limit the eccentricity is approaching zero, the adiabatic requirement that $\omega_r$ remain much less than the Kepler frequency is not violated because the strength of the effective field (and hence $\omega_s$) is decreasing more rapidly as $1/r_2^2$.

The analytic theory derived from the coupled single-electron models provides an illuminating explanation of the shape-preserving orbits in Fig. 2(b), but even for cases in which $\gamma$ is not equal to zero the preceding analysis provides insight into the dynamics. Figure 5(a) shows a single-electron orbit closely matched to the helium orbit in Fig. 1(c). In these orbits there is a sinusoidal exchange of angular momentum that in the case of helium produces a nonuniform angular velocity of the outer electron. The magnitude of this angular velocity oscillates sinusoidally at the same frequency as the angular momentum exchange. Also, instead of adiabatically following the outer electron, the major axis of the inner electron's orbit now oscillates about a line connecting the nucleus and the outer electron. As can be seen from Figs. 1(c) and 5, many features of these multielectron orbits are explained by the coupled one-electron models but a more general approach will be required to produce quantitative agreement.

An obvious extension to the shape-preserving orbits described in the preceding section is to include configurations in which the outer electron is in an elliptical orbit with eccentricity $\epsilon_2$. In this case the rotational frequency of the outer electron will vary around the orbit, as will the effective electric field. To first order both of these quantities vary as $1/r_2^2$, causing the ratio of $\omega_s/\omega_r$ to remain constant, thus maintaining the condition $\gamma=0$. The constancy of this ratio was pointed out by Bellomo *et al.* [27] who used this fact to develop a simple geometrical interpretation of collisional population of high angular momentum Rydberg states.

This result would seem to indicate that the condition for stable orbits, Eq. (13), might still be satisfied even when the outer orbit is elliptical. The adiabatic theory is easily modified to include these cases. At a radius $r_2$, the angular frequency of the outer electron is given by

$$\omega_r=\frac{l_2}{r_2^2}. \tag{19}$$

Reexpressing $l_2$ in terms of $Z_{\mathrm{eff}}$, $\epsilon_2$, and $r_2$ we find an expression analogous to Eq. (18):

$$\frac{3E_{\mathrm{eff}}(r_2)}{2Z}=-\frac{e_1}{l_1}\sqrt{\frac{(1-\epsilon_2)Z_{\mathrm{eff}}(r_2)}{r_2^3}}. \tag{20}$$

We can solve this in a manner identical to that used for circular outer orbits and we find that, for a given inner electron orbit, there is a complete set of elliptical orbits for the outer electron. In Fig. 6 we show these results for an inner orbit of $\epsilon_1=0.68$.

The numerical simulations reveal that these predicted orbits are not a simple extension of the previous shape-preserving orbits. The failure of this prediction lies in the assumption that the effective electric field was approximately Coulombic. Equation (17) provides a more accurate expres-

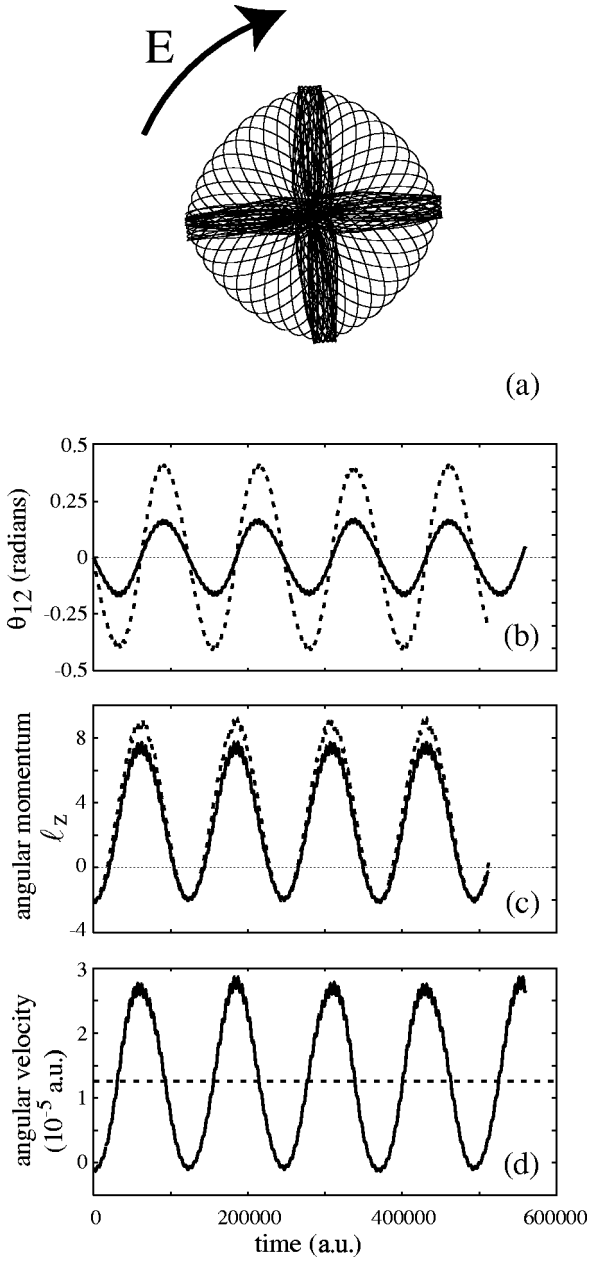


FIG. 5. (a) This classical one-electron orbit in a rotating electric field corresponds to the two-electron orbit shown in Fig. 1(c). The three plots compare (b) the angle between the major axis of the inner electron's orbit and the outer electron or field, (c) the angular momentum of the inner electron, and (d) the angular velocity of the outer electron or field. The solid lines represent the two-electron model and the dashed lines are the results of the hydrogenic atom in a rotating field.

sion for this field in which the higher-order terms are not negligible for any eccentricity $\epsilon_1$. The higher-order terms in the multipole expansion lead to a precession of the outer orbit that is analogous to the precession seen in alkali atoms [34]. More eccentric orbits will experience a more rapid precession because of the enhanced ''core'' effects at small radii.

Despite the presence of these non-Coulombic effects, the predicted configurations are approximately shape preserving, even for quite eccentric orbits of the outer electron. This adiabatic model reveals the nature of this class of *double ring* [13] orbits and explains why the exchange of angular momentum is small (though nonzero).

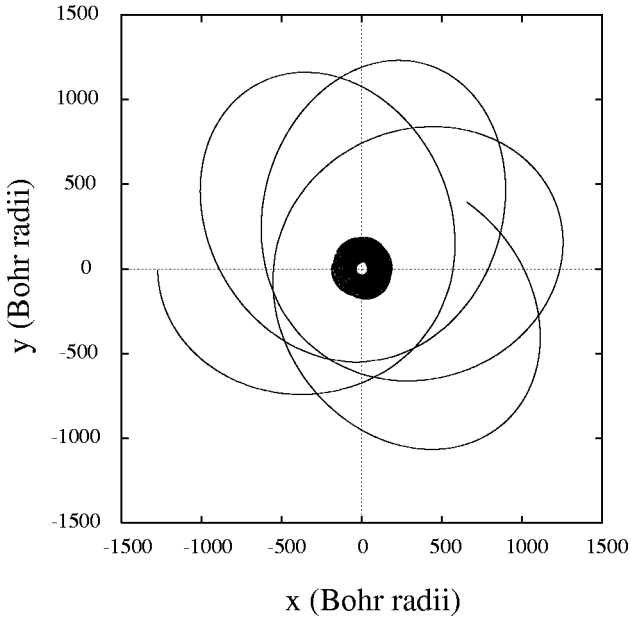


FIG. 6. A numerical simulation involving a noncircular orbit for the outer electron. The two-electron orbit is not of the shape-preserving class because of the higher order moments in the expansions of the effective core and effective electric field. These corrections lead to a precession of the orbit of the outer electron. The eccentricities of the inner and outer orbits are $\epsilon_1 = 0.68$ and $\epsilon_2 = 0.5$. The maximum exchange of angular momentum was $\Delta l = 3.6$.

## IV. QUANTUM-MECHANICAL CORRESPONDENCE

The calculations that we have carried out thus far make use of classical theory. In single-electron atoms, wave-packet states have bridged the gap between classical and quantum mechanics. Although in general, two-electron wave packets require the full two-electron quantum theory we can demonstrate the behavior of the shape-preserving orbits using hydrogenic quantum theory. The analysis of a classical electron interacting with a circularly polarized field did not depend on the exact initial position and momentum, but rather on the initial orbital parameters. The time averages in Eqs. (4) can be replaced by ensemble averages and Eqs. (9) can now be interpreted in terms of an ensemble of electrons rather than in terms of one isolated electron.

A quantum-mechanical analog of such a classical ensemble traveling in an elliptic orbit is an elliptic state [35]. Formally an elliptic state in the $xy$ plane is a coherent state in the rotation group in three dimensions, SO(3), whose generators are two components of the scaled Runge-Lenz operator, $\hat{A}_x$ and $\hat{A}_y$, and a component of the angular momentum, $\hat{L}_z$. These operators form a generalized angular momentum vector $\hat{\boldsymbol{\lambda}}$ whose classical analog is $\boldsymbol{\lambda}_{\parallel}$.

We will show that elliptic states do display behavior identical to that of a classical ensemble in a rotating electric field and, moreover, the elliptic state whose shape is stable in the field is an eigenstate in this field.

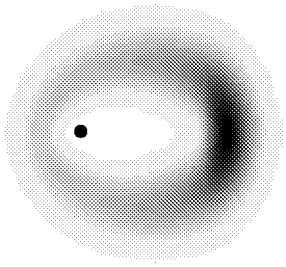

FIG. 7. The probability density of an elliptic state ($n=15$ and $\alpha=0.2\pi$) projected on to the $xy$ plane. The probability of finding an electron is greater in the neighborhood of the outer than in the neighborhood of the inner turning point. This state corresponds to $\langle\hat{\mathcal{L}}_z\rangle=11.33$ and an eccentricity of $\varepsilon=0.55$.

### A. Quantum theory of hydrogen in a weak rotating electric field

The derivation in Sec. II was a purely classical calculation but Eqs. (9) and Eq. (13) can be obtained quantum mechanically for a weak dc electric field in which neighboring $n$ manifolds are not mixed.

Using the Pauli substitution [36] we can write the Hamiltonian operator for an atom in a rotating electric field as

$$\hat{H}=\hat{H}_0-\boldsymbol{\omega}_s(t)\cdot\hat{\mathbf{A}}. \tag{21}$$

For a field rotating in the $xy$ plane, only the evolution of the operators associated with the classical vector $\lambda_{\|}$ is required. The Heisenberg equations of motion for $\hat{A}_x,\hat{A}_y$, and $\hat{L}_z$ are given by

$$\begin{aligned}
\frac{d}{dt}\hat{A}_x(t)&=-i[\hat{A}_x,\hat{H}]=-\omega_s\hat{L}_z\sin(\omega_r t),\\
\frac{d}{dt}\hat{A}_y(t)&=-i[\hat{A}_y,\hat{H}]=\omega_s\hat{L}_z\cos(\omega_r t),\\
\frac{d}{dt}\hat{L}_z(t)&=-i[\hat{L}_z,\hat{H}]=\omega_s[\hat{A}_x\sin(\omega_r t)-\hat{A}_y\cos(\omega_r t)],
\end{aligned} \tag{22}$$

where we have used the commutator relations for $\hat{A}_x,\hat{A}_y$, and $\hat{L}_z$.

We define operators $\hat{\mathcal{A}}_x$, $\hat{\mathcal{A}}_y$, and $\hat{\mathcal{L}}_z$ which are rotating with the field. The resulting operator equations of motion are *identical* in form to Eqs. (9) with $\tilde{A}_x,\tilde{A}_y$, and $\tilde{L}_z$ replaced by their operator equivalents. In order to reproduce the shape-preserving orbit quantum mechanically, the expectation values of these equations must reduce to Eqs. (9). The choice for the initial state is critical but we will show that the appropriate choice is an elliptic state.

The elliptic states may be represented as nongeometric rotations of the circular state $|n,n-1,n-1\rangle$ [37,38]

$$|\Psi(t)\rangle=e^{-i\alpha\hat{A}_y}|n,n-1,n-1\rangle. \tag{23}$$

The angle $\alpha$ parametrizes the rotation to produce the entire range of elliptic states whose major axes lie along the $x$ axis. The projection of the probability density of an elliptic state onto the $xy$ plane is shown in Fig. 7. The wave function is tightly localized about an ellipse whose eccentricity $\varepsilon$ is defined by

$$\varepsilon\equiv\langle\hat{A}_x\rangle/n=\frac{n-1}{n}\sin\alpha. \tag{24}$$

There exists a one-to-one correspondence between the classical orbits and the elliptic states whose parameters are related by

| quantum | $\leftrightarrow$ | classical |
|---|---|---|
| $\varepsilon$ | | $\frac{n-1}{n}\epsilon$ |
| $\langle\hat{L}_z\rangle$ | | $\frac{n-1}{n}L_z$. |

(25)

In the limit of large $n$, the scaling factor becomes unity and the expectation value of the quantum angular momentum and eccentricity are identical to the classical values. However, we will not require the invocation of the limit of large quantum numbers and the following derivation applies to all elliptic states regardless of $n$.

Choosing the elliptic state to be the initial state, the initial conditions are given by [35]

$$\begin{aligned}
\langle\hat{\mathcal{L}}_z(0)\rangle&=(n-1)\cos\alpha,\\
\langle\hat{\mathcal{A}}_x(0)\rangle&=(n-1)\sin\alpha,\\
\langle\hat{\mathcal{A}}_y(0)\rangle&=0.
\end{aligned} \tag{26}$$

The resulting time evolution of the expectation values of $\hat{\mathcal{A}}_x,\hat{\mathcal{A}}_y$, and $\hat{\mathcal{A}}_z$ is

$$\begin{aligned}
\langle\hat{\mathcal{L}}_z(t)\rangle&=(n-1)\cos\alpha+\frac{\omega_s}{\Omega^2}\gamma_q[\cos(\Omega t)-1],\\
\langle\hat{\mathcal{A}}_x(t)\rangle&=(n-1)\sin\alpha-\frac{\omega_r}{\Omega^2}\gamma_q[\cos(\Omega t)-1],\\
\langle\hat{\mathcal{A}}_y(t)\rangle&=\frac{\gamma_q}{\Omega}\sin(\Omega t),
\end{aligned} \tag{27}$$

where we have defined a quantum analog to $\gamma$ given by

$$\gamma_q=\omega_s(n-1)\cos\alpha+\omega_r(n-1)\sin\alpha. \tag{28}$$

When $\gamma_q=0$, the quantum state remains unchanged in the rotating frame just as in the classical orbits. The condition on the stabilizing field can be written as

$$\omega_s=-\omega_r\tan\alpha, \tag{29}$$

which can be shown to be equivalent to Eq. (13) using Eqs. (26)

$$\omega_r=-\frac{\omega_s\langle\hat{\mathcal{L}}_z(0)\rangle}{n\varepsilon(0)}. \tag{30}$$

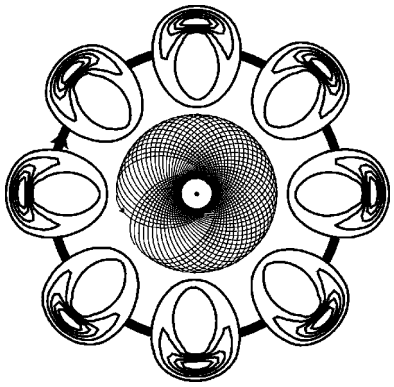

FIG. 8. This figure is a schematic representation of the correspondence between a rotating hydrogenic elliptic state (represented by the outer contour plots) and a classical helium orbit (inner trajectory). The elliptic state ($\alpha=0.238\pi$) evolves in a rotating field which satisfies Eq. (29). These snapshots in time reveal a shape-preserving wave packet that is exactly analogous to the shape-preserving classical orbit. The field strength is 2284V/cm and $\omega_r=1.08\times10^{-5}$. The elliptic state is in fact rotating about the nucleus contained within the contours but each snapshot has been displaced for illustrative purposes.

In Figs. 8 and 9 we show the evolution of a hydrogenic elliptic state in rotating electric fields. These snapshots of the evolution were obtained by numerically integrating Schrödinger's equation in the rotating field. The calculation involved only the $n=15$ manifold in hydrogen and the field strengths and frequencies were chosen to correspond to the equivalent case shown in Fig. 3 where $Z=2$. Note the correspondence to the classical orbit, which is perhaps most striking in Fig. 9 when compared to Fig. 3(b). The quantum state evolves identically to the classical orbit, its angular localization closely matching the eccentricity of the classical ellipse.

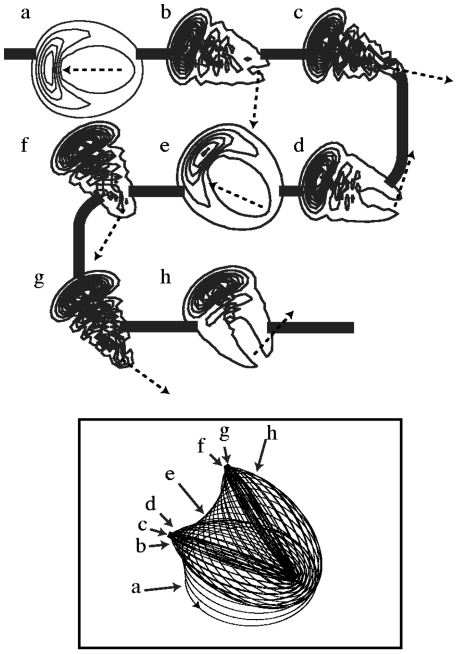


FIG. 9. Snapshots of the evolution of a hydrogenic ($Z=1$) elliptic state corresponding to $\langle\hat{\mathcal{L}}_z\rangle=10.26$ in a rotating electric field. The field does *not* satisfy (29) and the field strength is 2284V/cm and $\omega_r=-2.16\times10^{-5}$. The dashed arrows show the direction of the rotating field at the time of the snapshot and they clearly show that the wave packet does not follow the electric field.

Because of the difference in the classical and quantum definitions of the eccentricities [see Eqs. (25)], the conditions given by Eqs. (13) and (30) lead to slight differences in the initial conditions of the quantum and classical systems. In the limit of large $n$ the agreement is exact, but for modest values of $n$ the discrepancies are noticeable. For the example shown in Fig. 8 with $n=15$, the ratio $\omega_r/\omega_s$ is 1.08, leading to classical initial conditions of $l=11$ and $\epsilon=0.68$ but quantum initial conditions of $\langle\hat{\mathcal{L}}_z\rangle=10.27$ and $\varepsilon=0.64$.

### B. Eigenstate of rotating field

When the coherent state Eq. (23) is used as an initial wave function, we find that the wave function of the state will remain unchanged except for a rotation. We will now explicitly show that this state is in fact an eigenstate in this rotating field [39,40].

We choose as an initial state the elliptic state represented by Eq. (23). The Hamiltonian for the case of a hydrogen atom interacting with a right-circularly polarized field in a rotating frame is [41]

$$\hat{\mathcal{H}}=\hat{\mathcal{H}}_0-\omega_r\hat{\mathcal{L}}_z-\omega_s\hat{\mathcal{A}}_x, \tag{31}$$

where we have rewritten the interaction term using the Pauli substitution. The usual time-evolution operator is rewritten as

$$\hat{U}(t,0)=e^{-i\omega_r t\hat{\mathcal{L}}_z}e^{-it(\hat{\mathcal{H}}_0-\omega_r\hat{\mathcal{L}}_z-\omega_s\hat{\mathcal{A}}_x)}, \tag{32}$$

leading to a time evolution of the elliptic states of

$$\begin{aligned}|\psi_n(t)\rangle&=\hat{U}(t,0)|\psi_n(0)\rangle\\&=e^{-i\omega_r t\hat{\mathcal{L}}_z}e^{-it(\hat{\mathcal{H}}_0-\omega_r\hat{\mathcal{L}}_z-\omega_s\hat{\mathcal{A}}_x)}e^{-i\alpha\hat{\mathcal{A}}_y}|n,n-1,n-1\rangle.\end{aligned} \tag{33}$$

With the aid of the commutation relations and standard operator algebra, the product of exponentials can be reduced using

$$\begin{aligned}e^{i\alpha\hat{\mathcal{A}}_y}(\hat{\mathcal{H}}_0-\omega_r\hat{\mathcal{L}}_z-\omega_s\hat{\mathcal{A}}_x)e^{-i\alpha\hat{\mathcal{A}}_y}&\\=\hat{\mathcal{H}}_0+\hat{\mathcal{L}}_z(\omega_r\cos\alpha-\omega_s\sin\alpha)&\\+\hat{\mathcal{A}}_x(\omega_s\cos\alpha+\omega_r\sin\alpha).&\end{aligned} \tag{34}$$

When the condition $\omega_r\sin\alpha+\omega_s\cos\alpha=0$ is satisfied, operator $\hat{\mathcal{A}}_x$ vanishes from Eq. (33). Note that this condition is the same as Eq. (29). The state at time $t$ is then

$$\begin{aligned}|\psi_n(t)\rangle&=e^{-i\phi(t)}e^{-i\omega_r t\hat{\mathcal{L}}_z}(e^{-i\alpha\hat{\mathcal{A}}_y}|n,n-1,n-1\rangle),\\&=(\text{phase})\times(\text{rotation})\times(\text{initial state}),\end{aligned} \tag{35}$$

where $\phi(t)=t/2n^2+t(\omega_r\cos\alpha-\omega_s\sin\alpha)(n-1)$ is the time-dependent phase. Equation (35) states that the wave function at time $t$ is just the initial elliptic state rotating in step with

the applied field. In other words, an elliptic state is an eigenstate of the atom-plus-field Hamiltonian in the rotating frame, provided that the strength and rotational frequency of the field satisfy Eq. (30).

We have shown that the shape-preserving classical orbits have as analogs, the elliptic states, which are eigenstates of the circularly polarized electric field. The classical model offers a simpler system for studying the properties of the quantum states and it suggests possible approaches for exploring two-electron wave packets.

## V. CONCLUSIONS

In the orbits that we have described the coordinates and momenta of the two electrons are uncorrelated; instead the coordinates of one electron are correlated with the orbital parameters of the other electron. This classical result agrees with the observation that angular correlations dominate in doubly excited states while radial correlations are found only when the electronic wave functions have equal extent [16]. This indicates that explorations of wave-packet states and the classical limit of two-electron atoms might better utilize angularly localized wave packets [42] rather than the radial wave packets that have proven so useful in the case of one-electron atoms.

The experimental realization of such two-electron wave packets is not expected to be a simple matter. To observe the shape-preserving orbits one must excite a state that is essentially an elliptic state in the presence of a three-dimensionally localized circular orbit wave packet. Recently, two-electron Rydberg experiments have relied heavily on isolated core excitation [16] to achieve a multistep excitation of the final doubly excited state. The two-electron wave packets suggested here will require a similar stepwise approach in which wave packets, not eigenstates, are excited in individual electrons. By themselves, each of these single-electron wave packets represents a significant experimental challenge that must be met before such two-electron wave packets can be realized. The models discussed in this paper suggest that the production of circular orbit wave packets [43] in alkalis and studies of hydrogenic elliptic states in rotating fields are very important first steps that must be taken in order to develop the techniques required for two-electron wave packet experiments.

## ACKNOWLEDGMENTS

We would like to acknowledge helpful discussions with J. Bromage, J. D. Corless, M. F. VanLeeuwen, G. Ezra, and M. Kalinski. This work was supported in part by the U.S. Army Research Office.

[1] For a general review, see M. Nauenberg, C. R. Stroud, Jr., and J. Yeazell, Sci. Am. **270**, 24 (1994).
[2] I. C. Percival, Proc. R. Soc. London, Ser. A **353**, 289 (1977).
[3] R. S. Berry, Contemp. Phys. **30**, 1 (1989).
[4] T. Uzer, D. Farrelly, J. A. Milligan, P. E. Raines, and J. P. Skelton, Science **253**, 42 (1991).
[5] K. Richter, G. Tanner, and D. Wintgen, Phys. Rev. A **48**, 4182 (1993).
[6] J. A. West, Ph.D. thesis, University of Rochester, 1997.
[7] *Niels Bohr, Collected Works*, edited by J. R. Nielsen (North-Holland, New York, 1976), Vol. 3.
[8] J. H. van Vleck, Philos. Mag. **44**, 842 (1922); I. Langmuir, Phys. Rev. **17**, 339 (1921).
[9] M. C. Gutzwiller, *Chaos in Classical and Quantum Mechanics* (Springer-Verlag, New York, 1990).
[10] D. Wintgen and K. Richter, Comments At. Mol. Phys. **29**, 261 (1994).
[11] D. Wintgen, K. Richter, and G. Tanner, Chaos **2**, 19 (1992).
[12] H. A. Bethe and E. E. Salpeter, *Quantum Mechanics of One- and Two-Electron Atoms* (Plenum, New York, 1977).
[13] T. Yamamoto and K. Kaneko, Phys. Rev. Lett. **70**, 1928 (1993).
[14] K. Richter and D. Wintgen, Phys. Rev. Lett. **65**, 1965 (1990).
[15] F. Benvenuto, G. Casati, and D. L. Shepelyansky, Phys. Rev. A **53**, 737 (1996).
[16] T. Gallagher, *Rydberg Atoms* (Cambridge University Press, New York, 1994).
[17] V. N. Ostrovsky and N. V. Prudov, J. Phys. B **28**, 4435 (1995); Phys. Rev. A **51**, 1936 (1995).
[18] Z. D. Gaeta and C. R. Stroud, Jr., Phys. Rev. A **42**, 6308 (1990); Z. D. Gaeta, Ph.D. thesis, University of Rochester, 1995.
[19] U. Eichmann, V. Lange, and W. Sandner, Phys. Rev. Lett. **64**, 274 (1990).
[20] P. A. Braun, V. N. Ostrovsky, and N. V. Prudov, Phys. Rev. A **42**, 6537 (1990).
[21] V. N. Ostrovsky, Phys. Rev. A **46**, R5309 (1992); J. Phys. B **26**, 1163 (1993).
[22] K. Richter, J. Briggs, D. Wintgen, and E. Solov'ev, J. Phys. B **25**, 3929 (1992).
[23] I. C. Percival and D. Richards, J. Phys. B **12**, 2051 (1979).
[24] J. C. Solem, Am. J. Phys. **55**, 906 (1987).
[25] L. C. Biedenharn, L. S. Brown, and J. C. Solem, Am. J. Phys. **56**, 661 (1988).
[26] T. P. Hezel, C. E. Burkhardt, M. Ciocca, L-W. He, and J. J. Leventhal, Am. J. Phys. **60**, 329 (1992); **60**, 324 (1992).
[27] P. Bellomo, D. Farrelly, and T. Uzer, J. Chem. Phys. **107**, 2499 (1997).
[28] Such approximations pervade physics under various guises. For examples in celestial mechanics, see D. Hestenes, *New Foundations for Classical Mechanics* (Reidel, Dordrecht, Netherlands, 1986). In solid state physics a rudimentary discussion can be found in N. W. Ashcroft and N. D. Mermin, *Solid State Physics* (Saunders College Publishing, New York, 1976).
[29] Quantum mechanical two-electron systems could support more complex shape-preserving wave packets based on classical orbits which do not share the same orbital plane.
[30] M. Kalinski, J. H. Eberly, J. A. West, and C. R. Stroud, Jr. (unpublished).
[31] I. Bialynicki-Birula, M. Kalinski, and J. H. Eberly, Phys. Rev.

Lett. **73**, 1777 (1994); M. Kalinski, J. H. Eberly, and I. Bialynicki-Birula, Phys. Rev. A **52**, 2460 (1995); M. Kalinski and J. H. Eberly, *ibid.* **52**, 4285 (1995); **53**, 1715 (1996).

[32] D. Farrelly and T. Uzer, Phys. Rev. Lett. **74**, 1720 (1995); E. Lee, A. F. Brunello, and D. Farrelly, Phys. Rev. A **55**, 2203 (1997); A. F. Brunello, T. Uzer, and D. Farrelly, *ibid.* **55**, 3730 (1997).

[33] I. Bialynicki-Birula and Z. Bialynicki-Birula, Phys. Rev. Lett. **77**, 4298 (1996).

[34] J. A. West and C. R. Stroud, Jr., Opt. Express **1**, 35 (1997).

[35] J. C. Gay, D. Delande, and A. Bommier, Phys. Rev. A **39**, 6587 (1989).

[36] Quantum mechanically, Pauli showed that $\hat{\mathbf{r}} = -(3n/2Z)\hat{\mathbf{A}}$. Classically, the same result relates the time-averaged radius vector to the time-averaged scaled Runge-Lenz vector. The classical result is used in the derivation of Eqs. (4). W. Pauli, Z. Phys. **36**, 336 (1926); reprinted in English in *Sources of Quantum Mechanics*, edited by B. L. van der Waerden (Dover Publications, Inc., New York, 1967), p. 387.

[37] A. M. Perelomov, Commun. Math. Phys. **26**, 22 (1972).

[38] A. M. Perelomov, *Generalized Coherent States and Their Applications* (Springer-Verlag, Berlin, 1986).

[39] D. Wintgen, Z. Phys. D **18**, 125 (1991).

[40] M. Nauenberg, in *Coherent States: Past Present and Future*, edited by D.-H. Feng (World Scientific Publishing Co., River Edge, 1994).

[41] W. Salzman, Chem. Phys. Lett. **25**, 302 (1974).

[42] J. A. Yeazell and C. R. Stroud, Jr., Phys. Rev. A **35**, 2806 (1987); Phys. Rev. Lett. **60**, 1494 (1988).

[43] Z. D. Gaeta, M. W. Noel, and C. R. Stroud, Jr., Phys. Rev. Lett. **73**, 636 (1994).